ChemComm

ROYAL SOCIETY OF CHEMISTRY

COMMUNICATION

View Article Online
View Journal



Cite this: DOI: 10.1039/d6cc01851c

Received 26th March 2026,
Accepted 24th April 2026

DOI: 10.1039/d6cc01851c

rsc.li/chemcomm

# Bioinspired total synthesis of (dibromo)sceptrin and (dibromo)ageliferin†

Mohammed Latrache, [a] Amina Sesay, [a] Samuel Oger, [a] Mireia Benito Montaner, [b] Mohamed Mellah, [c] Erwan Poupon, [a] Stephen T. Hilton, [b] Stellios Arseniyadis [d] and Laurent Evanno *[a]

**We report a bioinspired synthesis of the emblematic marine alkaloids sceptrin, dibromosceptrin, ageliferin and dibromoageliferin. Central to this approach is a photocatalytic dimerization of fully elaborated precursors *via* [2+2] or [4+2] cycloadditions in batch and in flow. Notably, this work constitutes the first total syntheses of these natural products achieved by direct assembly of the native hymenidin and oroidin frameworks.**

The pyrrole–imidazole alkaloids (PIAs) are a family of natural products derived from oroidin-like precursors.[1–3] Its emblematic congener, oroidin (**1**), first isolated, is a major metabolite from *Agelas* spp. Sponges (Fig. 1).[4] Sceptrin (**3**),[5] the first reported dimeric PIA, was isolated in 1981 from *Agelas sceptrum* and arises from a [2+2] head-to-head dimerization of hymenidin (**1**).[6] Soon after, ageliferin (**4**) was the first [4+2] PIA cycloadduct isolated.[7] Their complex structures have made them central targets in total synthesis, inspiring numerous synthetic studies.[8–16] The first racemic syntheses of sceptrin (**3**) were independently reported by Baran[8] and Birman.[9] Baran constructed the central cyclobutane *via* fragmentation of a 3-oxaquadricyclane, whereas Birman used a classical [2+2] assembly between malonic anhydride and 1,4-dichlorobut-2-ene. Later, Baran and co-workers developed an asymmetric version of their synthesis using an enzymatic desymmetrization of a *meso*-oxaquadricyclane intermediate.[10] In 2014, Chen and co-workers synthesized (−)-sceptrin *via* a photocatalytic [2+2] cycloaddition of a chiral diene derived from D-glutamic acid.[11] For ageliferin (**4**), Chen employed a $Mn(OAc)_3$-mediated oxidative radical cyclization to forge the central core,[13] while Harran used a spirocyclic ring expansion.[14] Notably, Baran and co-workers prepared ageliferin (**4**) by simply heating sceptrin (**3**) in water under microwave irradiation.[15]

To date, sceptrin (**3**) and ageliferin (**4**) stand as emblematic examples of natural [2+2] and [4+2] cycloadducts, suggesting a biomimetic synthetic approach. While such disconnections have enabled the total synthesis of many complex molecules,[17,18] the direct biomimetic conversion of the complete core of hymenidin (**2**) into complex natural dimers **3** and **4** has remained elusive despite Jamison's significant contribution.[19] This limitation notably arises from the challenges associated with applying photocycloaddition conditions to highly functionalized and photosensitive substrates such as **1** and **2**. Under conventional batch photochemical conditions, prolonged irradiation leads to poor control, photodegradation, and competing side reactions. To overcome these intrinsic limitations of batch photochemistry, continuous-flow technology has emerged as a powerful alternative for conducting light-driven reactions.[20,21] In the context of photocatalysis, small-volume tubing eliminates dark zones inherent to batch systems, ensuring superior light penetration and uniform irradiation. Recently, Hilton and co-workers developed a low-cost, fully 3D-printed continuous-flow platform operated by compressed air or nitrogen.[22–26] Its modular design integrates photochemical reactors with in-line monitoring sensors, allowing precise control over flow rate, temperature, and irradiation parameters. By combining high reproducibility with an intuitive user-oriented design, this cost-effective setup significantly broadens access to flow photochemistry for the organic chemistry community. Building on these advantages, we applied this technology to the synthesis of four pyrrole–imidazole alkaloids, culminating in the first bioinspired synthesis of sceptrin (**3**) and ageliferin (**4**) from a complete hymenidin-like precursor, a long-standing challenge despite extensive efforts. Notably, the exclusive formation of head-to-head dimers supports a substrate-dependent biosynthetic assembly and provides experimental validation of a controlled, precursor-driven dimerization pathway.

Building on our previous work on aplysinopsins,[27,28] we aimed to develop a general photocatalytic approach to various natural products from oroidin (**1**) and hymenidin (**2**) (Fig. 1).

[a] *BioCIS, CNRS, Université Paris-Saclay, 91400, Orsay, France. E-mail: laurent.evanno@universite-paris-saclay.fr*
[b] *UCL School of Pharmacy, University College London, 29-39 Brunswick Square, WC1N 1AX, London, UK*
[c] *ICMMO, CNRS, Université Paris-Saclay, 91400, Orsay, France*
[d] *Queen Mary University of London, Department of Chemistry, Mile End Road, E1 4NS, London, UK*

† This work is dedicated to the memory of Professor Bernard Bodo, Professor at the Muséum National d'Histoire Naturelle, Paris.

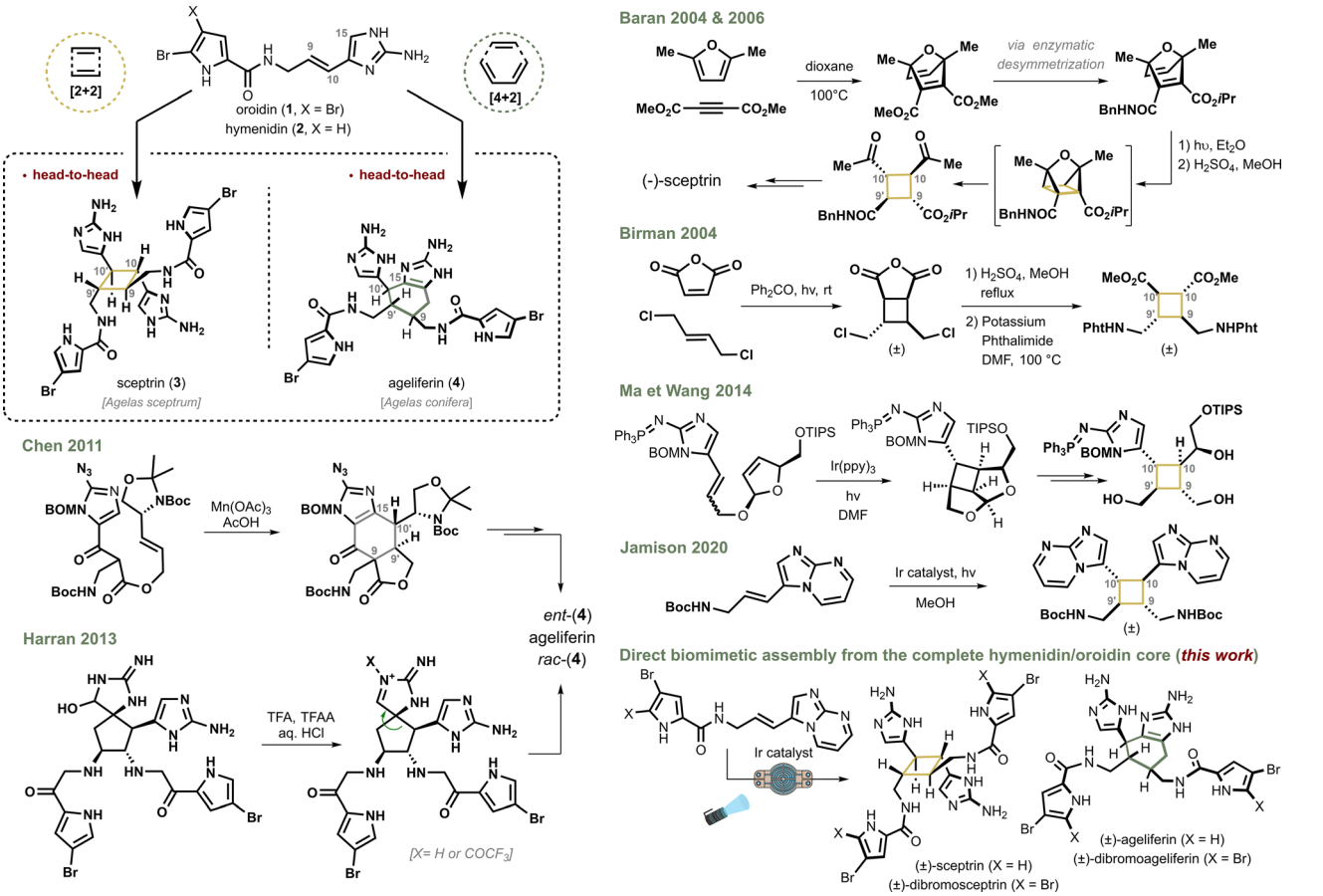


Fig. 1 Structure of sceptrin (**3**) and ageliferin (**4**) and reported synthetic strategies.

Photocatalytic [2+2] and [4+2] cycloadditions have been extensively described,[18,29–31] notably through radical cation cycloadditions of styrenes,[32–36] radical anion cycloadditions of acrylates,[37,38] or energy transfer mechanisms.[39–42] An extensive screening of ruthenium- and iridium-based photocatalysts was carried out on oroidin (**1**) and hymenidin (**2**), both prepared by adapting the synthesis reported by Rasapalli and co-workers (Fig. 2).[43] A diverse set of catalysts was employed, comprising $Ru(bpy)_3Cl_2$, $Ru(bpm)_3Cl_2$, $Ru(bpy)_2(dppz)(PF_6)_2$, $Ru(bpz)_3(PF_6)_2$, $[Ir(dtbbpy)(ppy)_2]PF_6$, $Ir[dF(CF_3)ppy]_2(dtbbpy)PF_6$ and *fac*-$Ir(ppy)_3$ previously used by Jamison and co-workers in their synthesis of the cyclobutane core of sceptrin. Attempts systematically resulted in rapid and complete degradation of the substrate. We therefore decided to run the reactions on the oroidin (**8**) and hymenidin (**9**) precursors instead, starting with the former. Following Molinski's observation that radical cations could be formed by cell-free enzyme preparations and promote C–C bond formation in the biosynthesis of PIA,[44] we first focused on oxidative conditions. We used the same set of ruthenium and iridium catalysts under a range of reaction parameters, including the presence of co-oxidants (methyl viologen dichloride, air, or anthracene) in a 2 : 1 mixture of acetonitrile and DMSO to solubilize the substrate. Hence, in the presence of $Ru(bpy)_3Cl_2$, $Ru(bpy)_2(dppz)(PF_6)_2$, *fac*-$Ir(ppy)_3$ or $Ir[dF(CF_3)ppy]_2(dtbbpy)PF_6$, a few oxidation products of **8** were isolated but no dimer was detected by HPLC-HRMS. Oxygenation products at C9, C10 and C15 were identified (see the SI for full details, Fig. S7). Interestingly, dimerization of compound **8** was efficiently promoted within minutes using *fac*-$Ir(ppy)_3$ or $Ir[dF(CF_3)ppy]_2(dtbbpy)PF_6$ under an inert atmosphere of argon (Table 1, entries 1 and 3). Notably, the addition of $iPr_2EtN$ (2.5 equiv.) in conjunction with *fac*-$Ir(ppy)_3$ led to a marked increase in conversion (Table 1, entry 4). Of the two catalysts, *fac*-$Ir(ppy)_3$ demonstrated superior efficiency in facilitating dimer formation. Four distinct dimeric structures were isolated from **8**: two arising from [2+2] cycloadditions (**10** and **14**) and two from formal [4+2] cycloadditions (**12** and **16**). Notably, product **10** features a sceptrin-like framework, whereas product **12** is a diastereomer likely formed *via E*/*Z* isomerization of one of the monomeric units prior to the cycloaddition. As for products **14** and **16**, they exhibit an ageliferin-type skeleton.

Reaction parameters, including solvent composition, catalyst loading, base concentration, and irradiation time, were systematically optimized (Table 1 and Table S8 in the SI). A reaction time of 60 min was identified as optimal; prolonged irradiation did not improve the yield and instead led to significant degradation. In a control experiment, the cyclobutane derivative **10** was irradiated with blue LEDs. After 2 min of irradiation in the presence of the catalyst, the reaction afforded a complex mixture composed of monomer **8**, cyclobutane dimers, and [4+2] cycloaddition products, all in comparable amounts, confirming the

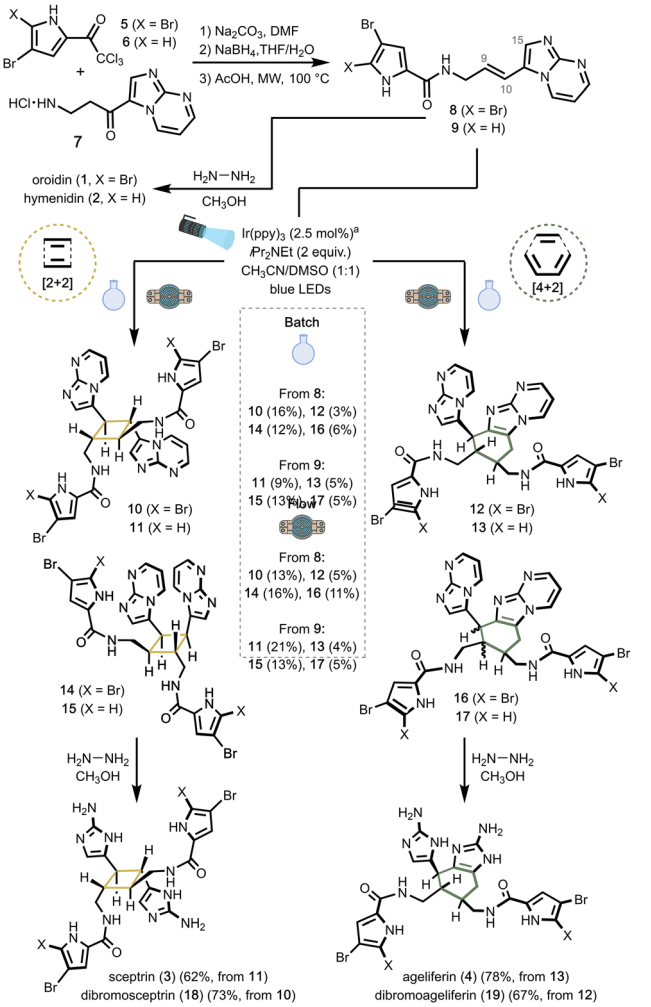


Fig. 2 Synthesis and dimerization of oroidin and hymenidin derivatives. [a] Catalyst loading was reduced to 1 mol% for the continuous-flow conditions.

reversibility of the process. On a preparative scale, the reaction time was adjusted to 80 min, and products **10**, **12**, **14** and **16** were isolated in 16%, 3%, 12% and 6% yield, respectively (37% cumulative yield). The same conditions were applied to the hymenidin-type substrate **9** (Fig. 2) delivering **11**, **13**, **15** and **17** in 9%, 5%, 13% and 5% isolated yield (32% cumulative yield). Notably, these reactions showed reproducibility issues, as minor variations in flask positioning relative to the light source occasionally affected conversion or led to product degradation. To complete the total syntheses, dimers **10**, **11**, **12** and **13** were reacted with hydrazine in methanol to afford dibromosceptrin (**18**, 73%), sceptrin (**3**, 62%), dibromoageliferin (**19**, 67%) and ageliferin (**4**, 78%), respectively.

Regarding the dimerization mechanism of the oroidin and hymenidin derivatives, we first hypothesized reductive quenching cycles since the use of $iPr_2EtN$ was necessary for the reactions to proceed. The electrochemical behavior of substrates **8** and **9** was evaluated by cyclic voltammetry in acetonitrile (see the SI for full details). The oxidation potentials of **8** ($E_{ox}$ = +2.50 V) and **9** ($E_{ox}$ = +2.40 V) were determined by cyclic voltammetry. No reduction waves were observed within the potential window of 0.0 to −3.5 V *vs.* SCE. The absence of detectable reduction events indicates that these substrates are not readily reduced under the conditions examined. We therefore considered a mechanistic scenario in which photoinduced oxidation of **8** or **9** by the excited state photocatalyst would initiate the dimerization. However, this pathway is thermodynamically unfavorable, as the excited-state oxidation potential of *fac*-Ir(ppy)$_3$ ($E_{p*/p^-} = +0.35$ V)[30] is insufficient to oxidize either substrate. Collectively, these electrochemical data are more consistent with an energy-transfer mechanism. In the absence of $iPr_2EtN$, low conversions were observed (Table 1, entry 3), whereas the addition of $iPr_2EtN$ brought the reactions to completion. We assume that the base interacts with the substrates to facilitate energy transfer rather than acting as an electron donor.

Following the identification of the most efficient photocatalytic systems, the study revealed several intrinsic limitations inherent to the batch conditions. The reaction proceeded in modest yields due to competing degradation and decomposition pathways. Moreover, the reaction suffered from reproducibility issues. Misalignments of the lamp caused fluctuations in yield, reflecting the narrow optimal irradiation window. To overcome these limitations, the optimized reaction conditions were implemented in a modular, 3D-printed continuous-flow system. This shift was driven by two key goals: first, to shorten the reaction times by achieving a more consistent and efficient photon distribution, and second, to improve the yields by reducing photodegradation caused by prolonged light exposure. The setup consists of modular reactor blocks connected in series. A nitrogen pressure propels the solvent through injection loops at typical flow rates between 0.1 and 1.0 mL min$^{-1}$, thereby obviating the need for mechanical pumps. Its narrow channels ensure uniform light penetration, avoiding dark zones and guaranteeing high reproducibility. The reactor is air-cooled and irradiated with a 456 nm Kessil® lamp. Residence time within the reactor is tunable *via* adjustment of the solvent flow rate and by configuring the system to include one or both of two reaction compartments, which can be linked in series. We employed a single injection loop containing a premixed solution of reactants and catalyst, with both reaction compartments connected in series.

The batch reactions involving substrates **8** and **9** displayed acceptable kinetics but afforded only modest cumulative yields (37 and 32%, respectively), largely due to significant degradation of both the starting materials and the products. To address this limitation, and drawing on our previous work on the bioinspired total synthesis of dimeric piperine alkaloids, we transitioned the reaction to PhotoFlow conditions.[45] In the case of the hymenidin-type substrate **9**, the batch conditions [*fac*-Ir(ppy)$_3$ (2.5 mol%), $iPr_2EtN$ (2.0 equiv.), and $CH_3CN$/DMSO (1 : 2) (0.23 mM)] were successfully translated to continuous flow. Hence, a residence time of 20 min at a flow rate of 0.1 mL min$^{-1}$ along with a lower catalyst loading (1 mol%) due to solubility issues afforded the sceptrin (**11**, 21%) and ageliferin **13** (4%) precursors, along with their isomers **15** (13%) and **17** (5%) in 43% cumulative yield. The same conditions applied to the oroidin derivative **8** yielded the dibromosceptrin (**10**, 13%) and dibromoageliferin **12** (5%) precursors, along with their isomers **14** (16%) and **16** (11%) in 45% cumulative yield. Interestingly, the PhotoFlow protocol enabled a reduction in irradiation time and catalyst loading

Table 1 Conditions for the [2+2] or [4+2] cycloadditions with **8**

| Entry | Catalyst | Conditions | Result[a] |
|---|---|---|---|
| 1 | $\{Ir(dFCF_3ppy)_2(dtbbpy)\}PF_6$ (5 mol%) | **8**, $CH_3CN$/DMSO (2 : 1) blue LEDs, 1 h | **10**: 6%; **12**: 2%<br>**14**: 7%; **16**: 1% |
| 2 | $\{Ir(dFCF_3ppy)_2(dtbbpy)\}PF_6$ (2.5 mol%)<br>blue LEDs, 5 h | **8**, $CH_3CN$/DMSO (2 : 1) $iPr_2EtN$ (1.0 equiv.) | **10**: 2%; **12**: 3%<br>**14**: 10%; **16**: 1% |
| 3 | *fac*-Ir(ppy)$_3$ (2.5 mol%) | **8**, $CH_3CN$/DMSO (1 : 1) blue LEDs, 1 h | **10**: 3%; **12**: 0%<br>**14**: 5%; **16**: 0% |
| 4 | *fac*-Ir(ppy)$_3$ (2.5 mol%) | **8**, $CH_3CN$/DMSO (1 : 1)<br>$iPr_2EtN$ (1.0 equiv.)<br>blue LEDs, 1 h | **10**: 10%; **12**: 3%<br>**14**: 12%; **16**: 1% |
| 5 | *fac*-Ir(ppy)$_3$ (2.5 mol%) | **8**, $CH_3CN$/DMSO (1 : 1) $iPr_2EtN$ (1.0 equiv.)<br>Blue LEDs, 1.5 h | **10**: 6%; **12**: 3%<br>**14**: 12%; **16**: 2% |
| 6 | *fac*-Ir(ppy)$_3$ (2.5 mol%) | **8**, $CH_3CN$/DMSO (1 : 1) $iPr_2EtN$ (2.0 equiv.)<br>Blue LEDs, 2 h | **10**: 8%; **12**: 4%<br>**14**: 10%; **16**: 1% |
| 7 | *fac*-Ir(ppy)$_3$ (2.5 mol%) | **8**, $CH_3CN$/DMSO (1 : 1)<br>$iPr_2EtN$ (1.0 equiv.)<br>blue LEDs, 2 h | **10**: 3%; **12**: 3%<br>**14**: 10%; **16**: 2% |
| 8 | *fac*-Ir(ppy)$_3$ (2.5 mol%) | **8**, $CH_3CN$/DMF (1 : 1)<br>$iPr_2EtN$ (1.0 equiv.)<br>blue LEDs, 1.5 h | **10**: 6%; **12**: 4%<br>**14**: 13%; **16**: 2% |

[a] Yields determined by HPLC analysis.

while markedly improving reproducibility, but didn't increase the overall yield unfortunately.

In summary, we successfully achieved the first reported assemblies of the complete hymenidin and oroidin scaffolds, enabling the bioinspired total synthesis of sceptrin, ageliferin, and their dibrominated congeners *via* [2+2] and [4+2] photocycloadditions, with only natural head-to-head dimers obtained. The use of a modular, cost-effective, 3D-printed continuous-flow system enabled reduced irradiation times, lower catalyst loading, and improved reproducibility.

## Conflicts of interest

There are no conflicts to declare.

## Data availability

All data supporting this study are provided in the supplementary information (SI). Supplementary information: experimental procedures, full screening results, compound characterisation, electrochemical measurements, and NMR spectra. See DOI: https://doi.org/10.1039/d6cc01851c.

## Acknowledgements

We thank the Agence Nationale de la Recherche (SMASH, ANR-2020-CE07-0021-01), Université Paris-Saclay, the CNRS, Queen Mary University of London and University College London for financial support and facilities. The authors thank Rémi Franco and Jean-Christophe Jullian for NMR assistance, and Karine Leblanc and Somia Rharrabti for LC-HRMS analyses.

## References

1 M. A. Beniddir, L. Evanno, D. Joseph, A. Skiredj and E. Poupon, *Nat. Prod. Rep.*, 2016, **33**, 820–842.
2 M.-J. Chu, M. Li, H. Ma, P.-L. Li and G.-Q. Li, *RSC Adv.*, 2022, **12**, 7789–7820.
3 M.-J. Chu, M. Li and Y. Zhao, *Bioorg. Chem.*, 2023, **133**, 106332.
4 S. Forenza, L. Minale, R. Riccio and E. Fattorusso, *J. Chem. Soc. D*, 1971, 1129–1130.
5 R. P. Walker, D. J. Faulkner, D. Van Engen and J. Clardy, *J. Am. Chem. Soc.*, 1981, **103**, 6772–6773.
6 J. Kobayashi, Y. Ohizumi, H. Nakamura and Y. Hirata, *Experientia*, 1986, **42**, 1176–1177.
7 P. A. Keifer, R. E. Schwartz, M. E. S. Koker, R. G. Hughes, D. Rittschof and K. L. Rinehart, *J. Org. Chem.*, 1991, **56**, 2965–2975.
8 P. S. Baran, A. L. Zografos and D. P. O'Malley, *J. Am. Chem. Soc.*, 2004, **126**, 3726–3727.
9 V. B. Birman and X.-T. Jiang, *Org. Lett.*, 2004, **6**, 2369–2371.
10 P. S. Baran, K. Li, D. P. O'Malley and C. Mitsos, *Angew. Chem., Int. Ed.*, 2006, **45**, 249–252.
11 Z. Ma, X. Wang, X. Wang, R. A. Rodriguez, C. E. Moore, S. Gao, X. Tan, Y. Ma, A. L. Rheingold, P. S. Baran and C. Chen, *Science*, 2014, **346**, 219–224.
12 T. Binh Nguyen, L. Anh Nguyen, M. Corbin, P. Retailleau, L. Ermolenko and A. Al-Mourabit, *Eur. J. Org. Chem.*, 2018, 5861–5868.
13 X. Wang, Z. Ma, J. Lu, X. Tan and C. Chen, *J. Am. Chem. Soc.*, 2011, **133**, 15350–15353.
14 H. Ding, A. G. Roberts and P. G. Harran, *Chem. Sci.*, 2012, **4**, 303–306.
15 P. S. Baran, D. P. O'Malley and A. L. Zografos, *Angew. Chem., Int. Ed.*, 2004, **43**, 2674–2677.
16 L. Barra and J. S. Dickschat, *Eur. J. Org. Chem.*, 2017, 4566–4571.
17 K. C. Nicolaou, S. A. Snyder, T. Montagnon and G. Vassilikogiannakis, *Angew. Chem., Int. Ed.*, 2002, **41**, 1668–1698.
18 D. Sarkar, N. Bera and S. Ghosh, *Eur. J. Org. Chem.*, 2020, 1310–1326.
19 L. V. Nguyen and T. F. Jamison, *Org. Lett.*, 2020, **22**, 6698–6702.
20 L. Wan, G. Kong, M. Liu, M. Jiang, D. Cheng and F. Chen, *Green Synth. Catal.*, 2022, **3**, 243–258.
21 L. Capaldo, Z. Wen and T. Noël, *Chem. Sci.*, 2023, **14**, 4230–4247.
22 M. R. Penny, Z. X. Rao, B. F. Peniche and S. T. Hilton, *Eur. J. Org. Chem.*, 2019, 3783–3787.
23 M. R. Penny and S. T. Hilton, *J. Flow Chem.*, 2023, **13**, 435–442.
24 J. Zhang, E. Selmi-Higashi, S. Zhang, A. Jean, S. T. Hilton, X. C. Cambeiro and S. Arseniyadis, *Org. Lett.*, 2024, **26**, 2877–2882.
25 M. B. Montaner and S. T. Hilton, *Curr. Opin. Green Sustainable Chem.*, 2024, **47**, 100923.
26 A. Hannam, P. Kankraisri, K. R. Thombare, P. Meher, A. Jean, S. T. Hilton, S. Murarka and S. Arseniyadis, *Chem. Commun.*, 2024, **60**, 7938–7941.
27 N. Duchemin, A. Skiredj, J. Mansot, K. Leblanc, J.-J. Vasseur, M. A. Beniddir, L. Evanno, E. Poupon, M. Smietana and S. Arseniyadis, *Angew. Chem., Int. Ed.*, 2018, **57**, 11786–11791.
28 S. Oger, N. Duchemin, Y. M. Bendiab, N. Birlirakis, A. Skiredj, S. Rharrabti, J.-C. Jullian, E. Poupon, M. Smietana, S. Arseniyadis and L. Evanno, *Chem. Commun.*, 2023, **59**, 4221–4224.

 

29 T. P. Yoon, *ACS Catal.*, 2013, **3**, 895–902.
30 C. K. Prier, D. A. Rankic and D. W. C. MacMillan, *Chem. Rev.*, 2013, **113**, 5322–5363.
31 D. A. Nicewicz and T. M. Nguyen, *ACS Catal.*, 2014, **4**, 355–360.
32 S. Lin, M. A. Ischay, C. G. Fry and T. P. Yoon, *J. Am. Chem. Soc.*, 2011, **133**, 19350–19353.
33 S. Lin, C. E. Padilla, M. A. Ischay and T. P. Yoon, *Tetrahedron Lett.*, 2012, **53**, 3073–3076.
34 M. Riener and D. A. Nicewicz, *Chem. Sci.*, 2013, **4**, 2625–2629.
35 S. M. Stevenson, R. F. Higgins, M. P. Shores and E. M. Ferreira, *Chem. Sci.*, 2016, **8**, 654–660.
36 K. Nakayama, N. Maeta, G. Horiguchi, H. Kamiya and Y. Okada, *Org. Lett.*, 2019, **21**, 2246–2250.
37 M. A. Ischay, M. E. Anzovino, J. Du and T. P. Yoon, *J. Am. Chem. Soc.*, 2008, **130**, 12886–12887.
38 J. Du and T. P. Yoon, *J. Am. Chem. Soc.*, 2009, **131**, 14604–14605.
39 L.-M. Zhao, T. Lei, R.-Z. Liao, H. Xiao, B. Chen, V. Ramamurthy, C.-H. Tung and L.-Z. Wu, *J. Org. Chem.*, 2019, **84**, 9257–9269.
40 E. M. Sherbrook, H. Jung, D. Cho, M.-H. Baik and T. P. Yoon, *Chem. Sci.*, 2020, **11**, 856–861.
41 E. M. Sherbrook, M. J. Genzink, B. Park, I. A. Guzei, M.-H. Baik and T. P. Yoon, *Nat. Commun.*, 2021, **12**, 5735.
42 M. J. Genzink, M. D. Rossler, H. Recendiz and T. P. Yoon, *J. Am. Chem. Soc.*, 2023, **145**, 19182–19188.
43 S. Rasapalli, V. Kumbam, A. N. Dhawane, J. A. Golen, C. J. Lovely and A. L. Rheingold, *Org. Biomol. Chem.*, 2013, **11**, 4133–4137.
44 E. P. Stout, Y.-G. Wang, D. Romo and T. F. Molinski, *Angew. Chem., Int. Ed.*, 2012, **51**, 4877–4881.
45 M. Latrache, A. Sesay, S. Oger, M. B. Montaner, J. Zhang, M. Mellah, E. Poupon, S. T. Hilton, S. Arseniyadis and L. Evanno, *Chem. Commun.*, DOI: 10.1039/D6CC01304J.